

Received March 16, 2021, accepted April 29, 2021, date of publication May 10, 2021, date of current version May 20, 2021.

Digital Object Identifier 10.1109/ACCESS.2021.3078799

Fully Inkjet-Printed Carbon Nanotube-PDMS-Based Strain Sensor: Temperature Response, Compressive and Tensile Bending Properties, and Fatigue Investigations

JOHANNES JEHN^{1,2,5}, PATRICK OSER², M. A. MAZ COURRAU^{1,2}, MICHAEL KAISER^{1,2}, DATONG WU^{1,2}, CHRISTIAN U. GROSSE^{1,3}, ULRICH MOOSHEIMER⁴, ANDREAS RUEDIGER⁵, AND CHRISTINA SCHINDLER^{1,2}

¹Laboratory for Microsystems Technology, Munich University of Applied Sciences, 80335 Munich, Germany

²Department of Applied Sciences and Mechatronics, Munich University of Applied Sciences, 80335 Munich, Germany

³Department of Civil Geo and Environmental Engineering, Technical University of Munich, 81245 Munich, Germany

⁴Laboratory for Print and Media Technology, Munich University of Applied Sciences, 80335 Munich, Germany

⁵Institut national de la recherche scientifique - Énergie Matériaux Télécommunications (INRS-EMT), Varennes, QC J3X 1S2, Canada

Corresponding author: Johannes Jehn (jehn@hm.edu)

This work was supported by the Hochschule München University of Applied Sciences and in part by the German Research Foundation (DFG) through the “Open Access Publishing” Program. The work of Andreas Ruediger was supported in part by the Ministère de l'Économie, Science et Innovation (MESI) Project and in part by the Natural Sciences and Engineering Research Council of Canada (NSERC). The work of Christina Schindler was supported by the NSERC.

ABSTRACT Printed and flexible sensors are in the focus of recent efforts to establish the advantages of low-cost manufacturing techniques such as screen printing or inkjet printing for printed electrical applications. Devices based on conductive carbon nanotube (CNT) networks within polymeric matrices such as polydimethylsiloxane (PDMS) are already exceeding mere technological demonstrations. Therefore, we investigate the application-oriented behaviour of fully inkjet-printed CNT/PDMS strain sensors under different conditions such as short- and long-term performance. The sensors exhibit a quasi-linear piezoresistive behaviour with vanishing hysteresis to tensile strain. Significant differences in the resistive response between compressive and tensile strain suggest complex re-orientation mechanisms of CNTs inside the matrix. No clear indication for this phenomenon could be observed in the evolution of the CNT network resistance during fatigue measurements within an uncured or cured PDMS matrix, where both scenarios exhibit no visual degradation. However, these measurements over thousands of cycles show different permanent changes in the overall device resistance exhibiting damages but also recovery in the network. Considering these findings facilitates the development of printed sensor devices.

INDEX TERMS Carbon nanotubes, inkjet printing, piezoresistivity, PDMS, strain sensor.

I. INTRODUCTION

Printed electronics has become more and more attractive as a complementary method to conventional silicon-based fabrication of electronic devices. This is due to new possibilities, including the usage of flexible, transparent substrates, high customizability and decentralized production. Inkjet printing as an additive deposition technique is already well established in the field of research and development owing to

The associate editor coordinating the review of this manuscript and approving it for publication was Chaitanya U Kshirsagar.

fast prototyping, low production costs, and less demanding production environments compared to cleanroom-based lithography processes. Further, printed electronics also allows for applications which require mechanical flexibility, such as strain gauges or biomedical devices.

Flexible sensor devices have attracted enormous interest and research efforts within the last years. Especially utilizing multi-walled carbon nanotubes (MWCNTs) as the sensing layer has developed rapidly from depositing CNT powder between adhesive tapes [1]. Nowadays, growing and filtering of CNTs enables obtaining conductive networks [2], [3],

using screen-printing [4], [5], or even inkjet printing [6] for CNT-based applications. Additionally, it has been shown recently that carbon electronics enables recyclable printed electronics with a recovery yield for of 95 % [7].

Recent research advances such as evaporation-driven self-assembly [8], [9] prove additional future potential for printed, CNT-based materials. Furthermore, new applications of inkjet-printed CNT films such as spatial strain sensing that can be utilized for damage detection [10] is fostering further research. Alternative approaches include conductive polymer composites (CPC), where the flexibility and strain properties of polymers are extended by conductive additives such as CNTs [11]. A recent review article gives a detailed and extensive overview on recent progress on piezoresistive strain sensors [12].

An especially promising material composition is found in the combination of MWCNTs with polydimethylsiloxane (PDMS). Here, the active material (MWCNT) is embedded in a PDMS matrix which can promote the adhesion to the substrate and creates an intrinsic stability for the conductive CNT network (CNN). This combination has been found to exhibit uniformly distributed MWCNTs enabling high performance flexible heating elements [13] or strain sensors with almost linear piezoresistive response to large strain levels of up to 40 % [14]. It even expands the possible applications as it encourages the use for health monitoring due the biocompatibility of PDMS [15].

Here, we demonstrate a fully inkjet-printable CNT-based temperature and strain sensor and investigate which role the curing process of PDMS plays regarding the long-term fatigue behaviour and how it could impact future applications.

II. METHODS

A. DEVICE FABRICATION

The synthesis of the inks used for inkjet printing in this work is based on recent research projects realising an inkjet-printed fibre-optic photoacoustic generator using MWCNTs in combination with PDMS [16], [17]. To facilitate the printing process and extend the shelf-life of the ink, a two-step printing process was chosen. The MWCNTs with an outer diameter of 6-9 nm and lengths around 5 μm are purchased from Sigma Aldrich (724769-100G). PDMS and the curing agent are commercially available from Dow Corning (Sylgard 184) where the latter is only used in the second step of the printing process. The first component (CNT/PDMS) is a water-based CNT-PDMS ink where polyoxyethylene octyl phenyl ether (Triton-X-100) is used to dissolve the CNTs in water and mediate CNTs and PDMS in the solution. The ratio of MWCNTs/PDMS is 1:3, therefore the dried ink contains a CNT content of ca. 25 wt%. The untreated constituents are homogenized for 30 minutes using a 130 W ultrasonic homogenizer. A solubility of 1 mg/ml of PDMS in a 0.1 % Triton-X-100 based on deionized water was found [16]. The second component (PDMS/CA) contains PDMS and the curing agent (CA) where an additional short chain PDMS acts

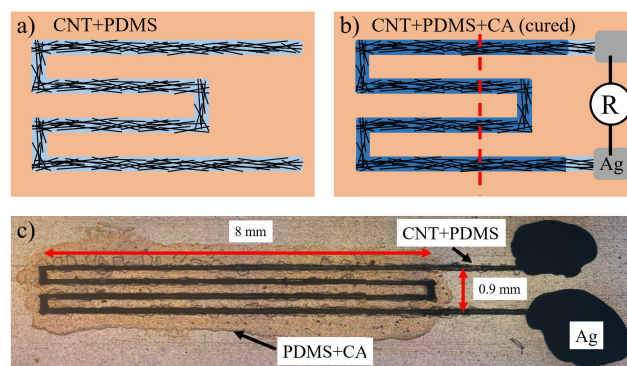


FIGURE 1. The printing process on polyimide substrate includes a) the application of the CNT/PDMS structure and after drying (100 °C, 10 minutes) follows b) printing of the curing agent (CA) and curing step (250 °C, 30 minutes) and Ag paste for contacting. The resistance is measured between the two contacts for the characterization and the red, dashed line indicates the bending axis. c) Stitched optical microscope image of final structure.

as a solvent. The undissolved parts of the PDMS/CA ink are homogenized for 2 minutes using a 130 W ultrasonic homogenizer [17]. The additional PDMS in the first component assists the homogeneous distribution of CNTs within the PDMS matrix which reduces separation between CNT and PDMS and promotes stability and adhesion to the substrate of the printed structures.

The sensors were fabricated by a two-step inkjet printing process using a Dimatix DMP 2831 inkjet printer. Initially, the 125 μm Kapton (polyimide) substrate is cleaned with 2-propanol to remove dust particles from it that could impair the printing process. In the first printing step, the drop-on-demand printer is applying the digitally designed pattern of the sensor using the CNT/PDMS ink with a drop spacing of 25 μm (Fig. 1 a). This inter-drop distance ensures a continuous line with minimal bulging. Multiple layers are achieved by repeating this printing process to reach a resistance in the desired range from 100 k Ω to 10 M Ω . The printed layers merge into each other as the evaporation time of the solvent is much longer than the time in between the application of multiple layers. After successful printing of the first step with several layers, the structure is heated on a hotplate at 100 °C for 10 minutes to get rid of residual solvents. At this stage, conductive Ag paste (Acheson 1415) is manually applied at the two ends of the sensor to measure the resistance and confirm the electrical conductivity of the CNT network.

For the second fabrication step, the sensor track is covered with PDMS/CA using a drop spacing of 25 μm (Fig. 1 b)). However, the areas at the two ends are covered with Ag paste to facilitate contacting. The amount of layers is adjusted to the number of CNT/PDMS layers to attain an overall appropriate ratio of PDMS and CA. A higher (lower) amount of CA leads to a more stiff (soft) cured PDMS matrix. Naserifar *et al.* [18] showed that inkjet printing of curing agent can be used to create local stiffness gradients in sub-mm-thick PDMS films. Therefore, we can assume that the printed CA in the second step will fully polymerize the previously applied PDMS/CNT

pattern. The final sensor is cured on a hotplate at 250 °C for 30 minutes to accomplish full polymerisation of the PDMS.

Additionally, a fully covered area of 8 × 8 mm² is printed to validate the electrical characterization, described in the next section. Unlike the printed lines for the sensor, this design is less prone to be affected by printing irregularities due to a lower demand in printing accuracy. Furthermore, this layout enables the characterization of the sheet and specific resistance of the CNT network via a four-probe measurement setup.

B. PHYSICAL AND ELECTRICAL CHARACTERIZATION

The length l of the sensor is determined by the print design given to the inkjet printer, yielding a total length of 34.6 mm. Electric measurements are performed using a Keithley 2400. One source of uncertainty arises as the start and end of the structure are covered with a conductive Ag paste to facilitate the electrical characterization. In order to calculate the resistivity $\rho_1 = R \cdot A/l$, where R is the electrical resistance and A the cross-section, the printed lines are measured before curing by profilometry (Veeco 150, 12.5 μm tip radius). This facilitates the measurement of A , as the curing layer covers wider parts of the substrate, making it difficult to determine the baseline. Here, curing refers to the processing step of adding the curing agent for cross-linking the PDMS chains. The evaluation of A is a major challenge due to the natural bending of the substrate. Even though the dimension of the bending is only in the range of μm, it is significant in comparison to the expected thickness of ca. 200–300 nm of the printed structure. However, since the lines have a width of <200 μm, this effect is taken care of by subtracting a linear background and characterizing a large sample size for a statistically significant value for A . As a secondary approach, the sheet resistance R_s of a fully printed CNT/PDMS square is measured using a four-point probe setup (Veeco FPP-100) to compare the influence of the curing process on R_s . Here, the thickness t is also measured by profilometry where the bending of the substrate can be fitted and subtracted.

For CNNs, the overall resistance is attributed to the summation of intrinsic resistance R_{CNT} , contact resistance R_C and tunneling resistance R_T [19]. This property will be of great importance for the discussion on the resistivity and the piezoresistive behaviour presented in sections III-B and III-D of the discussion.

C. EFFECTS OF PDMS CURING AND ALIGNMENT CONSIDERATIONS

After the first printing step, the structure consists of MWCNTs embedded in a not cross-linked PDMS matrix. In the last step, we investigate the effect of the curing process in the second printing step on the electrical and bending properties of the sensing CNT layer. For the electrical characterization, squares of (8 × 8) mm² are printed and measured before and after the application and curing using the curing agent. This design is chosen to detect possible re-alignments of the CNTs by measuring the resistance between opposite

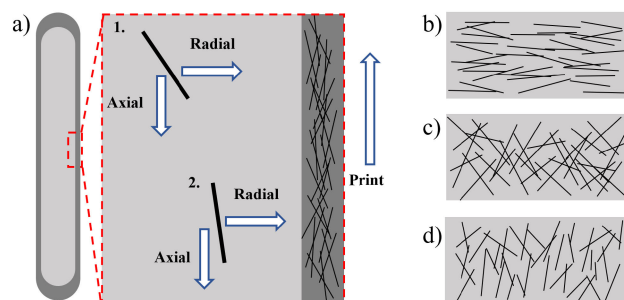


FIGURE 2. Schematics of possible CNT orientations. a) Flow-induced alignment of CNTs in the edge-accumulated coffee stain region, anti-parallel to the printing direction (adapted from [8], [21]). Orientations of a CNN with b) preferred horizontal, c) random and d) vertical orientation (adapted from [22]).

edges of the square during bending operations. Bending along the vertical axis could induce a change in the respective resistances. Initially, we expect some degree of alignment of CNTs along the horizontal printing direction. The deposited MWCNTs experience a radial force towards the periphery, exhibiting agglomeration at the fringes. This phenomenon is well known for inkjet printing and can be found in various fields as the coffee-ring effect [20]. Additionally, forces invoked by the solvent flux and van der Waals interactions between the CNTs cause parallel alignment to the printing direction (s. Fig. 2 a) [8]. Bending along the vertical axis could induce a re-orientation of the CNTs along this axis. This should be observable as a change in resistance along the horizontal or vertical direction, i.e., R_{hor} or R_{ver} , respectively (s. Fig. 2 b,d). On the one hand, a higher degree of alignment of the deposited CNTs should result in a smaller resistance, due to a lower number of contact resistances between the individual tubes [8]. On the other hand, alignment in a CNN results in a less random orientation, leading to minimized interconnection and thus to an increased electrical resistivity due to higher tunneling distances [21], [22].

Another benefit of the design is to probe the sheet resistance R_s , where the co-linear setup of the four-point prober has a width of ca. 4.5 mm. The probing needles are brought into contact with the sample in a light-protected station and can also pierce through the cured PDMS layer. Hence, changes of R_s due to the curing process can be evaluated.

D. TEMPERATURE SENSITIVITY

It is crucial for any practical application to determine the response of the system to environmental changes. Depending on the application, the device could be used as a temperature sensor itself or the cross-sensitivity during strain-sensing should be quantified. It is known that moisture can affect CNT/PDMS-based sensors [23]. For now, we disregard the influence of humidity on the sensoric properties.

We investigate the change in R with varying temperature steps of $\Delta T = 5$ °C in the range between 30 °C – 80 °C. The sample is put on a thermal chuck (WaferTherm SP 53 A) which is actively heated or cooled to the set point controlled

by a lab-built LabView program. The device temperature follows the change of the thermal chuck closely, as the substrate material is only $125 \mu\text{m}$ thick. Still, the measurement of R is taken by a Keithley 2400 sourcemeter with a waiting time of 5 s after the thermal chuck has reached its designated value to avoid thermal fluctuations. The temperature coefficient for resistance (TCR) is calculated as

$$TCR = \frac{\Delta R}{R_i} \cdot \frac{1}{\Delta T}, \quad (1)$$

where $\Delta R = R_f - R_i$ and ΔT are the differences between the final and initial resistance and temperature, respectively.

E. STRAIN TESTING SET-UP

For investigating the piezoresistive properties of our CNT-based sensor, we use a lab-built rotate-to-bend apparatus [24]. It allows customized sequences of tensile as well as compressive bending operations by a stepping motor. The latter has to be emphasized as many publications only report on tensile stress due to the difficulty to compress a flexible substrate in a controlled fashion. This can be overcome by utilizing our rotate-to-bend setup where the curvature during the rotation can be converted to a bending radius r as a function of [24]:

$$r(\beta) = L / \left(2\pi \sqrt{\left(1 - \sin\left(\frac{180^\circ - |\beta|}{2}\right)\right) - \frac{\pi^2 d^2}{12 \cdot L^2}} \right), \quad (2)$$

where β is the bending angle with respect to the neutral position which is positive for tensile and negative for compressive deformation, d is the thickness of the substrate and L is the spacing between the clamps holding the sample. The tensile or compressive strain ϵ is closely related to r by the formula $\epsilon = \pm d/(2r)$ [25].

The piezoresistive response to bending can be characterized in two ways: during a static bending measurement, the sample is bent step-wise and measurements are performed at defined bending angles in the bent state; for the fatigue test, the species performs full bending cycles (tensile, compressive, or both) with a certain maximum bending radius and is characterized at the neutral, unstrained position. This allows fast and reliable evaluation of the change in resistance during or after strain exposures. To comparatively quantify the sensitivity of the device, we calculate the gauge factor (GF)

$$GF = \frac{\Delta R}{R_i} \cdot \frac{1}{\epsilon}, \quad (3)$$

where $\Delta R = R_f - R_i$ is the difference between the final and initial resistance, respectively.

III. RESULTS AND DISCUSSION

A. MORPHOLOGY OF PRINTED STRUCTURES

An interesting observation in the printing behaviour of the CNT-based ink is a very brief settling phase in the beginning. By increasing the drop space, individual droplets can be created on the substrate. The initially applied drops are darker

in their visual appearance, before they become homogeneous after a few hundred μm . This implies that the first drops have a higher CNT concentration. Reasons for this could be a slight sedimentation after a resting period of the print head or a loss of solvent in the proximity to the ejection nozzles. Both incidents would lead to an increased CNT concentration of the first applied drops. A similar trend is reported by Dinh *et al.* [8], where they described a remarkable widening at the starting position of the lines and an agglomeration of MWCNTs. They interpret this as a sign for strong transportation against the printing direction due to an enhanced evaporation flux along the printed line to compensate the solvent loss at the contact line [8]. While this is an elegant way to explain the line shape and the phenomenon of CNT agglomeration, a higher density of CNTs in the first printed drops is not addressed. In our case the material flux cannot be the reason, as we do not have a continuous line. This behaviour should not affect any properties of the device as it occurs only in the first few drops. Similarly, Kao *et al.* [26] report an agglomeration of CNTs at the printing origin due to edge-enhanced evaporation and an overall decrease of CNT density along the printed lines. We do not observe such an extended trend for our printed structures.

Finally, to conclude the physical characterization, the adhesion and stability of the printed sensor is investigated. We successfully performed a self-adhesive tape test, where a strip of adhesive tape (tesafilm transparent, ca. $50 \mu\text{m}$) is applied and smoothed onto a cured sample line. The only visible change after the tape is pulled off is that the Ag paste has been partially removed. A small increase in resistance of ca. 1 % is observed after the removal of the tape which is within the measurement error of the multimeter (UT61B, $\pm 1 \%$). The same procedure leads to a complete removal of the film, if it is performed before the second printing, i.e., the curing step. This confirms that the PDMS content of the ink in the first printing step is not cross-linked to a significant degree and therefore cannot provide stability to the CNN structure before it is cured in the second step. It is noteworthy that even though the uncured sample is not resilient against external physical stresses, it exhibits no visible degradation or loss of adhesion during handling or bending operations.

B. ELECTRICAL CHARACTERIZATION

For a better understanding of the nature of the CNNs, sensors with different thicknesses are printed by modifying the layer count. Additional layers add more ink to the lines, resulting in a larger cross section A . For conventional conductive materials such as Cu or Ag, this would lead to a decrease in total resistance R . But the resistivity ρ would stay constant because it is an intrinsic material property. In the case of our structure, additional CNTs will not only contribute to the rise of A but also create a denser CNN which enhances the number of contact points between individual tubes. Unfortunately, we can neither measure the density nor degree of networking of the CNTs, as profilometry only probes the outline. We calculate $A = w \cdot t$, where w and t are the width and the average

TABLE 1. Cross-section A , resistance R , and resistivity ρ of CNT-based meanders for different number of printed layers. The uncertainty in R is negligible compared to the other values.

Nr. of Layers	A [10^{-11} m ²]	R [M Ω]	ρ [10^4 $\mu\Omega$ cm]
5	1.26 ± 0.52	3.28	12.0 ± 5.2
10	1.85 ± 0.76	1.86	10.0 ± 4.3
15	2.17 ± 1.27	1.12	7.0 ± 4.2
20	2.57 ± 1.32	0.56	4.2 ± 2.2

thickness of the structure, respectively. However, the change in ρ with increased number of layers and a subsequent growth of A is shown in Table 1. As expected, more applied material leads to a growth of A and decline of R . Still, ρ exhibits a clear downward trend. This does not imply that the individual CNTs become more conductive but that the CNN might develop into a denser mesh. The values for ρ are given in units of $\mu\Omega$ cm to compare them to conventional conductors that are in the range of 1.5–10 $\mu\Omega$ cm.

The large values for the errors in Table 1 are mainly induced by the uncertainties in the determination of t . Also, since the size of the probe is considerably larger than the roughness of the sample caused by the CNTs, the acquired result for A entails the convolution of the probe and the surface profile. This effect is well known for scanning force microscopy and will lead to an increase of the experimentally observed size of A , where the convolution error is enhanced for narrow objects [27]. We do not actively compensate the profilometry results for this effect because it is negligible in comparison to the effect of the substrate bending or its roughness.

Comparing our results to values found in the literature is difficult because ρ is often not given in publications or MWCNTs are mixed with other components such as epoxy or no binding material at all. Yan and Jeong [13] use solution-casting to fabricate a MWCNT/PDMS based electric heating element. The authors have measured ρ as a function of MWCNT content (wt%) and found a dramatic decrease from ca. 10^{13} $\mu\Omega$ cm for neat PDMS to ca. 10^6 $\mu\Omega$ cm for a 10 wt% composition of MWCNTs. Since our reported value is still at least one order of magnitude smaller, we can conclude that the further increase of MWCNT content in our inkjet-printed sensors (25 wt% compared to 10 wt%) results in a lower resistivity and agrees well with the detailed investigation by Yan *et al.* Another reference value is found in the work of Kao *et al.* [26] where they use a commercially available CNT ink (CNT-22, lab311, Korea) for a fully inkjet-printed strain sensor. Unfortunately, the exact composition of the ink is not disclosed and the thickness for a series of samples with different number of passes printed is not given. It is demonstrated that the sheet resistance is decreasing with the number of printed layers. Based on this observation, the authors claim that the “increase in the CNTs density [shows that] the sheet resistance decreased with the number of passes” [26]. However, by using the given sheet resistance and extrapolating the layer thickness from values given before in the paper, an

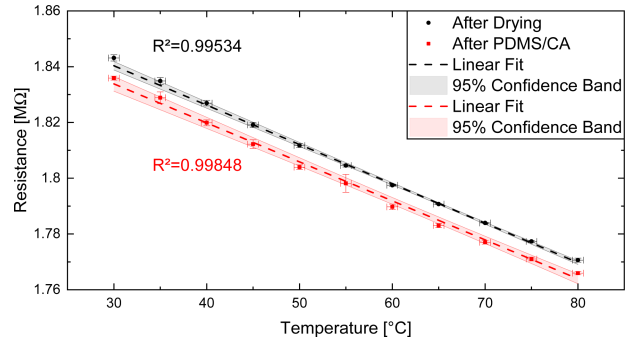


FIGURE 3. Thermoresistive behaviour of a CNT/PDMS sensor after drying the active material at 100 °C and after application of PDMS/CA and curing at 250 °C. The linear fits are shown with the corresponding 95 % confidence band.

TABLE 2. Parameters for linear fitting of data shown in Fig. 3 with the offset R_i and slope k . The temperature coefficient of resistance (TCR) is given with respect to $R(30^\circ\text{C})$.

Sample	R_i [M Ω]	k [$\Omega/^\circ\text{C}$]	TCR_{30} [%/ $^\circ\text{C}$]
After drying	1.876 ± 0.002	-1399 ± 32	-0.076 ± 0.002
After PDMS	1.883 ± 0.001	-1412 ± 18	-0.077 ± 0.001

almost constant resistivity of $\rho = (1.60 \pm 0.20) \cdot 10^5$ $\mu\Omega$ cm can be calculated. This is in the same range but still significantly higher than our reported value. We can therefore conclude that our reported values are among the highest for printed CNT-based structures and that we observe indications of densification of the CNN.

C. TEMPERATURE RESPONSE AND GAUGE FACTOR

The thermoresistive response of the CNT/PMDS is measured as described in section II-D to determine the temperature sensitivity. Fig. 3 shows the change in resistance for a temperature range between 30–80 °C. The first curve is taken after the first printing step, where the sample was treated with a temperature of 100 °C on a hotplate to get rid of solvent residues. The second curve is taken after the addition of a second layer with PDMS and CA and curing at 250 °C. Both curves exhibit almost identical initial resistances of 1.84 M Ω and a TCR of ca. -0.076 %/ $^\circ\text{C}$ (s. Table 2). The instrumental inaccuracy for the resistance measurement is negligible and is taken as $\pm 1^\circ\text{C}$ for the measured temperature. The error bars are calculated as the standard deviation from three individual, consecutive measurements and error propagation. The TCR is obtained by linear fitting of the thermoresistive behaviour according to Eq. 1 with respect to the initial resistance at $T=30^\circ\text{C}$.

This value is in the same order of magnitude as reported TCRs of CNT-based thermistors in the literature that span from -0.036 %/ $^\circ\text{C}$ (Epoxy/MWCNTs) [28] to -0.400 %/ $^\circ\text{C}$ (CNT) [29]. For established, metal-based, bonded strain gauges the TCR is in the order of $+0.001$ %/ $^\circ\text{C}$ [30].

D. BENDING PROPERTIES - STATIC AND FATIGUE

To determine the piezoresistive response of the CNT sensor and the long-term stability, the gauge factor (GF) is calculated and fatigue measurements are performed, respectively.

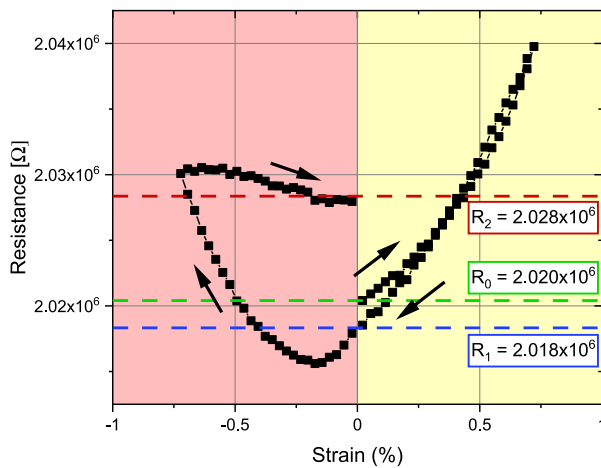


FIGURE 4. Piezoresistive behaviour for static bending of a cured CNT/PDMS sensor. The initial tensile strain ($\epsilon > 0$) causes a quasi-linear, hysteresis-free ($R_0 \approx R_1$) response with $GF = 1.40$. The subsequent compressive ($\epsilon < 0$) strain exhibits a more complicated behaviour, resulting in a permanent increase of R , with respect to the initial value ($R_2 > R_0$).

Fig. 4 shows a representative piezoresistive curve for static bending of a CNT/PDMS sensor. The values of the resistance at neutral position are labelled for descriptive and analytic purposes and are taken at the very beginning (R_0), after tensile bending (R_1) and in the end after compressive bending (R_2), respectively. The initial tensile bending towards a maximum strain of $\epsilon = 0.72\%$ and the return to the neutral position demonstrates a quasi-linear, hysteresis-free ($R_0 \approx R_1$) response with $GF \approx 1.4$. As a comparison, metal-based strain gauges have a GF of approximately 2 and a nominal resistance of ca. $100\ \Omega$ [30]. A higher initial resistance results in a larger absolute change in R , facilitating the read-out.

By mirroring this strain to the compressive regime $\epsilon = -0.72\%$, a more intricate behaviour is becoming apparent. Unlike for conventional, metallic strain gauges, the resistance does not decrease further. At $\epsilon \approx -0.2\%$ a sudden raise in R occurs, resulting in an increase even in the neutral position at R_2 . According to the Poisson effect, compression leads to transversal elongation resulting in a greater cross-section $A' > A$. The shortened $l' < l$ and expanded $A' > A$ should result in a lower absolute resistance R . However, this simplistic model holds only true for bulk materials. As described above, the strain sensing properties of CNNs are attributed to the summation of intrinsic resistance R_{CNT} , contact resistance R_C and tunneling resistance R_T and changes in the resistive properties are associated with modifications of contact arrangements and tunneling distances between CNTs [19]. We propose that the CNTs are gradually changing their alignment within the polymer matrix, especially during the compressive strain. It has been observed that an aligned network might actually increase the resistivity level, as the orientation of CNTs becomes less random, reducing the interconnection [21].

In the following, the two bending regimes are characterized individually. The sample is bent step-by-step to a maximum

strain of $\epsilon = \pm 1.0\%$ and returned to the original position. This is repeated several times for the same strain regime before switching to the opposite side (s. Fig. 5). By this, we want to investigate whether the peculiar behaviour for the compressive region observed in Fig. 4 is an effect originating in the previously applied strain. In Fig. 5 a), the tensile strain exhibits a quasi-linear response with a vanishing hysteresis after the third cycle. This demonstrates that this sensor could be used without concerns for tensile strain measurements after some initial bending cycles. The relative changes in Fig. 5 c) are calculated with respect to the initial resistance of the first measurement for R_0 and for each individual curve for the corresponding initial value of R_0 for R_1 and R_2 . It becomes apparent that some relaxation occurs after each measurement because the final resistance $R_{1,2}$ is always bigger than the initial resistance for the following measurement R_0 . Similar observations were reported for CNT-bases CPCs [31], [32]. There, increasing strain amplitudes led to a not fully recoverable increase in resistance and it is explained as a perpetual damage to the conductive network, as well as the microstructure of the viscoelastic polymer matrix.

For Fig. 5 b), subsequent compressive bending cycles exhibit a similar trend for a fading hysteresis effect, visible as the decline in the relative change of R_2 in Fig. 5 c). However, the characteristic rise at a certain strain level is always present, only shifting in its beginning from $\epsilon \approx -0.3\%$ for the first run, to $\epsilon \approx -0.6\%$ for the fourth run. Hereby, we can conclude that this general behaviour is not caused by a previous tensile bending but it is an intrinsic property of the CNT/PDMS sample.

The longevity of the sensor is investigated by measuring the resistance in neutral position after a repeated number of complete tensile-compressive bending cycles N . It is characterized after the first printing step where the ink only has been dried and with a different sample after the application of the curing agent and subsequent curing after the second printing step. As seen in Fig. 6, the degree of maximum strain to the system is given as the bending radius and in absolute strain percentage, calculated according to Eq. 2. The resistance R is measured every 10 cycles and the strain level is altered every 5000 runs. For lower strain amplitudes (here: $< 2\%$) the fatigue testing can be regarded as 'high-cycle fatigue' [33].

Fig. 6 shows several interesting trends that both curves have in common. Firstly, the resistance for strain levels of at least 0.72% increases significantly with repeated cycles. The increase exhibits a faster initial and larger absolute rise with growing strain levels, i.e., decreasing bending radii.

Secondly, lowering the absolute strain ($N > 20000$) exhibits an overall decreasing trend for the resistance. This is especially remarkable as a strain of 1.07% initially led to a sharp increase in R ($10000 < N < 20000$) while now it displays an overall decrease in R for ($20000 < N < 25000$). That is an indicator that the origin for the overall increase is not only a result of device deterioration but could be caused by re-orientation of CNTs in the PDMS matrix. In the case of crack evolution, further load should result in accumulation

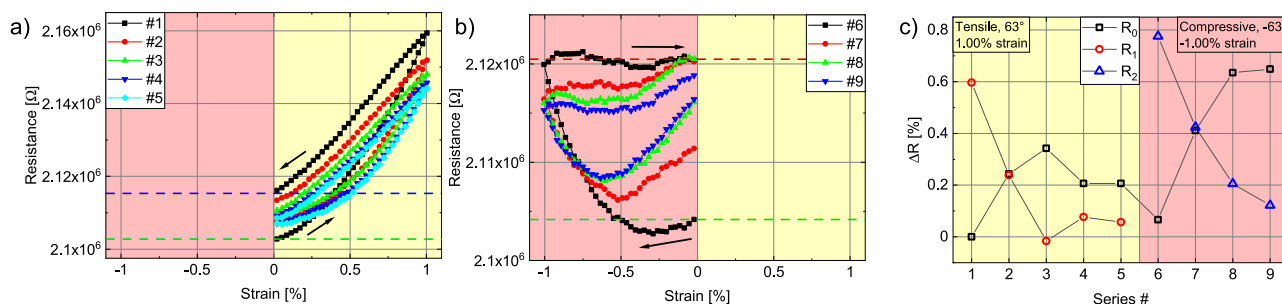


FIGURE 5. Piezoresistive behaviour of cured sensor for repeated tensile strain (a), compressive strain (b) and the relative variation (c) of the resistance after tensile and compressive strain (R_1 and R_2) with regard to the initial resistance of each measurement R_0 . The arrows in a) and b) indicate the direction of change and the dashed lines correspond to the values used in c).

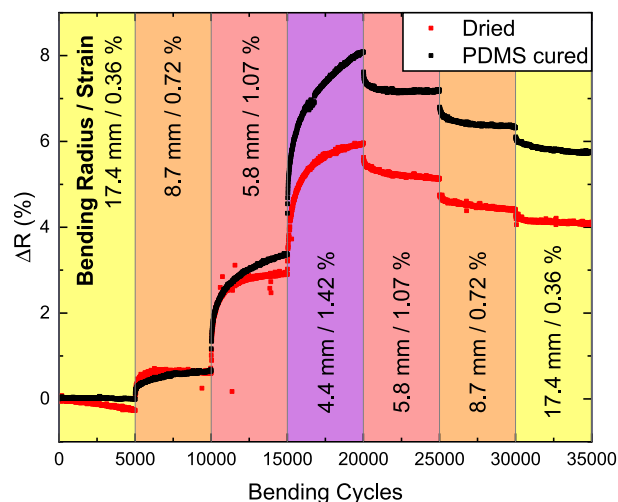


FIGURE 6. Endurance or fatigue measurement of a CNT/PDMS sensor after the first printing step (dried) and after the curing step (cured). The resistance is measured every 10 cycles in the neutral position after N complete tensile-compressive bending cycles under a certain bending radius and strain. The strain is changed every 5000 cycles.

of device damage, leading to a further increase of overall resistance. In the basic linear damage concept (Miner’s rule), the degree of damage to a sample is given by the ratio of work absorption per cycle and a characteristic amount of work absorbed at failure [34]. Therefore, each cycle of any load is linearly added to the total damage and would result in a strictly monotonous increase of resistance, which is not observed here. A related phenomenon was reported by Zhang *et al.*, where continuous (tensile) cycling with varying strain levels showed good recoverability after stabilization by cyclic loading. They also observed that lowering the strain level again, led to a recovery or even a decrease below the initial resistance. They concluded that this recovery is not only caused by the decrease in strain but also a time-dependent process. In our case, time-dependency cannot be excluded but the overall increase of R suggests a permanent change in the sensor.

A similar trend is visible for a strain of 0.72 %, where R exhibits an increase for a low-to-high loading sequence ($5000 < N < 10000$) but a reduction for a high-to-low

loading sequence ($25000 < N < 30000$). These considerations suggest, that the CNNs can compensate or heal deterioration over time which might be caused by re-orientation of CNTs. Hence, the mobility and movement of the CNTs induced by the high-to-low sequence enables energetically favourable CNT configurations, leading to a lower absolute resistance. For the lowest amount of strain 0.36 %, an initial slight decrease is visible for $0 < N < 5000$, indicating that the sample has been exposed to a higher load before the beginning of this fatigue test. Finally, the region $30000 < N < 35000$ displays no notable change but an overall increase compared to $N = 0$ of $\Delta R_{fat}(N) = 100 \cdot (R(35000) - R(0)) / R(0) = 4.1\%$ demonstrates that permanent damage is done to the sample.

However, the absolute change of the sensor in R differs significantly between the two printing steps. The final, cured sensor exhibits a more substantial increase, especially for the highest strain of 1.42 %. This rise is the main reason for the overall increase in R of ca. 5.8 % for the cured sample with respect to the initial value. The origin and effects of the cured PDMS layer will be discussed in the next section.

E. EFFECTS OF PROTECTIVE PDMS LAYER

To investigate the direct influence of the curing process on the resistance of the CNN, R_s is measured at six different positions on CNT squares with 5, 10 and 15 printed layers after both printing and curing steps. In Table 3, R_s is given for the averaged measurement results before and after curing. It is remarkable that R_s agrees well within the uncertainty boundary and therefore stays virtually unaffected by the curing process. This demonstrates, that neither the cross-linking process nor the high temperature step causes a macroscopic change for the network of CNTs. This result is not self-evident as the transition from uncured, gooeey PDMS to cured and solid PDMS might have come with significant changes within the CNN connections.

Finally, to evaluate the different responses between CNTs embedded in uncured and cured PDMS, an additional fatigue test is performed. It is conducted similar to the one described in Sec. III-D and shown in Fig. 6. Full tensile and compressive bending cycles along the vertical axis are carried out with the

TABLE 3. The sheet resistance $R_{s,l}$ for a CNT square of (8×8) mm² of various layers l after the first and second processing step. The first step contains printing of different layers of CNT/PDMS and drying at 100°C for 10 minutes, the second step includes printing of PDMS/CA and curing at 250°C for 30 minutes.

Printing step	$R_{s,5}$ [kΩ/sq.]	$R_{s,10}$ [kΩ/sq.]	$R_{s,15}$ [kΩ/sq.]
After drying	6.76 ± 0.98	3.00 ± 0.40	1.89 ± 0.20
After PDMS	7.37 ± 1.12	2.88 ± 0.21	1.96 ± 0.24

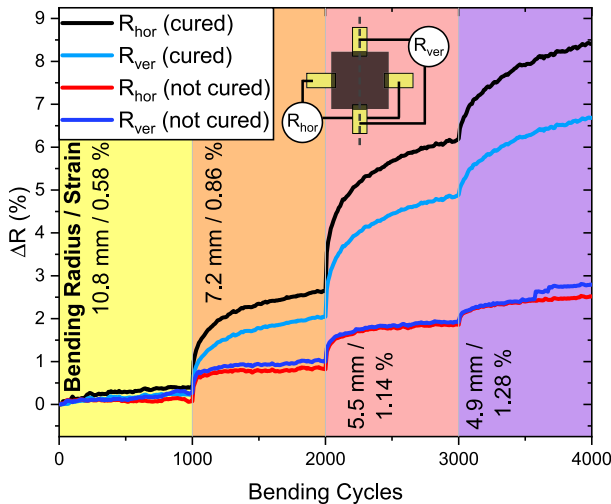


FIGURE 7. Fatigue measurement of a CNT-based sensor within an uncured and cured PDMS matrix. The resistance is measured every 10 cycles in the neutral position along the bending axis R_{ver} and perpendicular to it R_{hor} . After N complete tensile-compressive bending cycles under a certain bending radius and strain. The strain is changed every 1000 cycles. The inset shows the measurement configuration and the grey, dashed line indicates the bending axis.

TABLE 4. Initial resistances of printed CNT square before and after curing of PDMS along the horizontal and vertical direction, as seen in the inset of Fig. 7.

	R_{hor} [kΩ]	R_{ver} [kΩ]
Uncured	1.535	1.746
Cured	1.778	1.876

CNT-squares. This time, additionally to the measurement of R_{hor} as before, the resistance along the bending axis R_{ver} is determined every ten cycles. Every 1000 cycles, the strain is progressively increased. To avoid contacting problems, the square is printed on top of Au contacts of 200 nm that have been thermally deposited on the substrate. The contacts are positioned at the centre of all four edges of the CNT-square with an overlap in width of ca. 2 mm and depth of ca. 0.5 mm (Fig. 7, inset).

Fig. 7 shows a similar trend as Fig. 6, where increased strain causes a steeper growth in overall resistance. It shows the relative change of R over number of full bending cycles in the neutral position ($\Delta R = (R - R_0)/R_0$).

The comparison between the changes in R_{ver} and R_{hor} exhibit important differences in the uncured and cured state. As given in Table 4, R_{ver} is significantly higher than R_{hor} ,

indicating some alignment along the vertical printing direction. Shown in Fig. 7, the uncured device exhibits a change of 2–3 % in R after the complete procedure, while R of the cured device rises ca. 7–8 % for the same treatment. This could be caused by a difference between the soft, uncured PDMS matrix and the firm, cured matrix. The possible formation of micro-cracks or cavities might lead to a permanent increase in R . In the uncured case, these effects will not occur due the missing intrinsic stability.

This hypothesis is supported by the variance of R_{ver} and R_{hor} for the different PDMS states. The measurements for the uncured sample display basically the same development with increasing number of bending cycles and strain. However, for the cured structure, R_{hor} rises significantly more than R_{ver} . In the case of crack formation, defects would arise along the bending axis, i.e., perpendicular to the direction of measurement. These cracks would not affect R_{ver} as they run along the electric pathway. Therefore, the difference between R_{ver} and R_{hor} suggests the formation of cracks along the bending direction.

IV. LIMITATIONS OF THE STUDY AND OUTLOOK

Before we conclude, a few limitations of the presented study should be pointed out and how they will be addressed in the future. For a better understanding of the cross section A of the sensors, measurements via atomic force microscopy could be performed. Dinh *et al.* [8] used this approach for observing the coffee stain effect of CNNs without PDMS. Also, the orientation and possible re-alignment of CNTs due to bending was only probed indirectly via the electrical resistance. A more direct way could be taken by means of scanning electron microscopy which enables the observation of the orientation of CNTs after different treatments. Furthermore, for the longevity estimation of the sensor we used an accelerated process. In applications with sporadic but enduring utilization, resting periods and changes in the environment such as temperature and humidity need to be tested as well. Finally, it might be possible to investigate the effect of different levels of curing of PDMS on the sensoric performance. This could be achieved by varying the amount or content of curing agent in the second processing step.

V. CONCLUSION

We presented CNT/PDMS-based temperature and strain sensors and addressed application-related questions, such as the morphology, electrical properties, and their cross-sensitivity. The sensors exhibit a TCR of ca. $-0.076 \text{ \%}/^\circ\text{C}$ and a quasi-linear response to tensile strain with a gauge factor of ≈ 1.4 , making it a viable candidate for applications as a strain gauge with only a small temperature dependence. The GF is comparable to commercial strain gauges ($\text{GF} \approx 2$) but benefiting from an easier read-out due to the larger absolute change in R . The bending properties exhibited two distinct responses to tensile and compressive strain, respectively, where a quasi-linear response and a more intricate behaviour was observed. Fatigue measurements with 35 000 full bending cycles of

different strains showed a permanent increase in resistance which cannot be explained by the linear accumulation of device damage. The cured, stabilizing PDMS matrix showed no influence on the electrical conductivity of the CNN but accelerates a permanent rise of R , which is a sign of degradation. Considering all of these observations, we can conclude that no convincing indications for CNT alignment within the PDMS are present in the change of R . If it was, it should occur in the uncured PDMS matrix, where the CNTs are less fixed to their position compared to the solid, cured PDMS matrix. These findings provide a great asset to the development of further CNT/PDMS sensors. It demonstrates that the cured PDMS does not affect the conductivity of the CNN but it reduces the longevity by a more pronounced change in resistance during long-term applications. Therefore, the stiffness of the PDMS matrix should be controlled by applying varying amounts of curing agent to the sensor. In this way, desired material properties can be engineered depending on the application. Furthermore, the cured PDMS layer is necessary for protection against physical interactions such as touching or scratching even though the uncured sample already withstands handling and bending operations. These findings provide many novel and relevant insights for the fabrication of printed sensors.

REFERENCES

- [1] K. S. Karimov, F. A. Khalid, M. T. S. Chani, A. Mateen, and M. A. Hussain, "Carbon nanotubes based flexible temperature sensors," *Optoelectron. Adv. Mater. Rapid Commun.*, vol. 6, nos. 1–2, pp. 194–196, 2012.
- [2] A. Di Bartolomeo, M. Sarno, F. Giubileo, C. Altavilla, L. Iemmo, S. Piano, F. Bobba, M. Longobardi, A. Scarfato, D. Sannino, A. M. Cucolo, and P. Ciambelli, "Multiwalled carbon nanotube films as small-sized temperature sensors," *J. Appl. Phys.*, vol. 105, no. 6, Mar. 2009, Art. no. 064518.
- [3] X. Song, S. Liu, Z. Gan, Q. Lv, H. Cao, and H. Yan, "Controllable fabrication of carbon nanotube-polymer hybrid thin film for strain sensing," *Microelectron. Eng.*, vol. 86, no. 11, pp. 2330–2333, Nov. 2009.
- [4] S. Walczak and M. Sibiński, "Flexible, textronic temperature sensors, based on carbon nanostructures," *Bull. Polish Acad. Sci. Tech. Sci.*, vol. 62, no. 4, pp. 759–763, Dec. 2014.
- [5] K. Kanao, S. Harada, Y. Yamamoto, W. Honda, T. Arie, S. Akita, and K. Takei, "Highly selective flexible tactile strain and temperature sensors against substrate bending for an artificial skin," *RSC Adv.*, vol. 5, no. 38, pp. 30170–30174, 2015.
- [6] F. Michelis, L. Bodelot, Y. Bonnassieux, and B. Lebental, "Highly reproducible, hysteresis-free, flexible strain sensors by inkjet printing of carbon nanotubes," *Carbon*, vol. 95, pp. 1020–1026, Dec. 2015.
- [7] N. X. Williams, G. Bullard, N. Brooke, M. J. Therien, and A. D. Franklin, "Printable and recyclable carbon electronics using crystalline nanocellulose dielectrics," *Nature Electron.*, vol. 4, no. 4, pp. 261–268, Apr. 2021.
- [8] N. T. Dinh, E. Sowade, T. Blaudeck, S. Hermann, R. D. Rodriguez, D. R. Zahn, S. E. Schulz, R. R. Baumann, and O. Kanoun, "High-resolution inkjet printing of conductive carbon nanotube twin lines utilizing evaporation-driven self-assembly," *Carbon*, vol. 96, pp. 382–393, Jan. 2016.
- [9] G. L. Goh, S. Agarwala, and W. Y. Yeong, "Aerosol-Jet-Printed preferentially aligned carbon nanotube twin-lines for printed electronics," *ACS Appl. Mater. Interfaces*, vol. 11, no. 46, pp. 43719–43730, Nov. 2019.
- [10] Y. Zhao, S. Gschossmann, M. Schagerl, P. Gruener, and C. Kralovec, "Characterization of the spatial elastoresistivity of inkjet-printed carbon nanotube thin films," *Smart Mater. Struct.*, vol. 27, no. 10, Oct. 2018, Art. no. 105009.
- [11] X. Wang, J. Li, H. Song, H. Huang, and J. Gou, "Highly stretchable and wearable strain sensor based on printable carbon nanotube layers/polydimethylsiloxane composites with adjustable sensitivity," *ACS Appl. Mater. Interface*, vol. 10, no. 8, pp. 7371–7380, Feb. 2018.
- [12] L. Duan, D. R. D'hooge, and L. Cardon, "Recent progress on flexible and stretchable piezoresistive strain sensors: From design to application," *Prog. Mater. Sci.*, vol. 114, Oct. 2020, Art. no. 100617.
- [13] J. Yan and Y. G. Jeong, "Multiwalled carbon nanotube/polydimethylsiloxane composite films as high performance flexible electric heating elements," *Appl. Phys. Lett.*, vol. 105, no. 5, Aug. 2014, Art. no. 051907.
- [14] X. Fu, M. Ramos, A. M. Al-Jumaily, A. Meshkinzar, and X. Huang, "Stretchable strain sensor facilely fabricated based on multi-wall carbon nanotube composites with excellent performance," *J. Mater. Sci.*, vol. 54, no. 3, pp. 2170–2180, Feb. 2019.
- [15] C. Gerlach, D. Krumm, M. Illing, J. Lange, O. Kanoun, S. Odenwald, and A. Hubler, "Printed MWCNT-PDMS-Composite pressure sensor system for plantar pressure monitoring in ulcer prevention," *IEEE Sensors J.*, vol. 15, no. 7, pp. 3647–3656, Jul. 2015.
- [16] P. Oser, O. Düttmann, F. Schmid, L. Schulte-Spechtel, C. U. Große, and D. Wu, "Synthesis and characterization of CNT composites for laser-generated ultrasonic waves," *Macromol. Mater. Eng.*, vol. 305, no. 4, Apr. 2020, Art. no. 1900852.
- [17] P. Oser, J. Jehn, M. Kaiser, O. Düttmann, F. Schmid, L. Schulte-Spechtel, S. S. Rivas, C. Eulenkamp, C. Schindler, C. U. Grosse, and D. Wu, "Fiber-optic photoacoustic generator realized by inkjet-printing of CNT-PDMS composites on fiber end faces," *Macromol. Mater. Eng.*, vol. 306, no. 2, Feb. 2021, Art. no. 2000563.
- [18] N. Naserifar, S. S. Yerneni, L. E. Weiss, and G. K. Fedder, "Inkjet printing of curing agent on thin PDMS for local tailoring of mechanical properties," *Macromol. Rapid Commun.*, vol. 41, no. 5, Mar. 2020, Art. no. 1900569.
- [19] W. Obitayo and T. Liu, "A review: Carbon nanotube-based piezoresistive strain sensors," *J. Sensors*, vol. 2012, pp. 1–15, Feb. 2012.
- [20] R. D. Deegan, O. Bakajin, T. F. Dupont, G. Huber, S. R. Nagel, and T. A. Witten, "Capillary flow as the cause of ring stains from dried liquid drops," *Nature*, vol. 389, no. 6653, pp. 827–829, Oct. 1997.
- [21] S. Abbasi, P. J. Carreau, and A. Derdouri, "Flow induced orientation of multiwalled carbon nanotubes in polycarbonate nanocomposites: Rheology, conductivity and mechanical properties," *Polymer*, vol. 51, no. 4, pp. 922–935, Feb. 2010.
- [22] K. Parmar, M. Mahmoodi, C. Park, and S. S. Park, "Effect of CNT alignment on the strain sensing capability of carbon nanotube composites," *Smart Mater. Struct.*, vol. 22, no. 7, Jul. 2013, Art. no. 075006.
- [23] K. Leemets, U. Mäeorg, A. Aabloom, and T. Tamm, "Effect of contact material and ambient humidity on the performance of MWCNT/PDMS multimodal deformation sensors," *Sens. Actuators A, Phys.*, vol. 283, pp. 1–8, Nov. 2018.
- [24] B. Huber, J. Schober, M. Kaiser, A. Ruediger, and C. Schindler, "Rotate-to-bend setup for fatigue bending tests on inkjet-printed silver lines," *Flexible Printed Electron.*, vol. 3, no. 3, Aug. 2018, Art. no. 035005.
- [25] J. Lewis, "Material challenge for flexible organic devices," *Mater. Today*, vol. 9, no. 4, pp. 38–45, Apr. 2006.
- [26] H.-L. Kao, C.-L. Cho, L.-C. Chang, C.-B. Chen, W.-H. Chung, and Y.-C. Tsai, "A fully inkjet-printed strain sensor based on carbon nanotubes," *Coatings*, vol. 10, no. 8, p. 792, Aug. 2020.
- [27] J. Canet-Ferrer, E. Coronado, A. Forment-Aliaga, and E. Pinilla-Cienfuegos, "Correction of the tip convolution effects in the imaging of nanostructures studied through scanning force microscopy," *Nanotechnology*, vol. 25, no. 39, Sep. 2014, Art. no. 395703.
- [28] H. C. Neitzert, L. Vertuccio, and A. Sorrentino, "Epoxy/MWCNT composite as temperature sensor and electrical heating element," *IEEE Trans. Nanotechnol.*, vol. 10, no. 4, pp. 688–693, Jul. 2011.
- [29] V. S. Turkani, D. Maddipatla, B. B. Narakathu, B. J. Bazuin, and M. Z. Atashbar, "A carbon nanotube based NTC thermistor using additive print manufacturing processes," *Sens. Actuators A, Phys.*, vol. 279, pp. 1–9, Aug. 2018.
- [30] Omega Engineering Inc. (2021). *Omega Kfh Series: Pre-Wired Strain Gages (Data Sheet)*. [Online]. Available: <https://assets.omega.com/pdf/test-and-measurement-equipment/strain-gauges/KFH.pdf>
- [31] R. Zhang, H. Deng, R. Valencia, J. Jin, Q. Fu, E. Bilotti, and T. Peijs, "Strain sensing behaviour of elastomeric composite films containing carbon nanotubes under cyclic loading," *Compos. Sci. Technol.*, vol. 74, pp. 1–5, Jan. 2013.
- [32] J. Chen, Y. Zhu, and W. Jiang, "A stretchable and transparent strain sensor based on sandwich-like PDMS/CNTs/PDMS composite containing an ultrathin conductive CNT layer," *Compos. Sci. Technol.*, vol. 186, Jan. 2020, Art. no. 107938.

- [33] J. Schijve, "Fatigue of structures and materials in the 20th century and the state of the art," *Int. J. Fatigue*, vol. 25, no. 8, pp. 679–702, Aug. 2003. [Online]. Available: <http://www.sciencedirect.com/science/article/pii/S0142112303000513>
- [34] A. Fatemi and L. Yang, "Cumulative fatigue damage and life prediction theories: A survey of the state of the art for homogeneous materials," *Int. J. Fatigue*, vol. 20, no. 1, pp. 9–34, Jan. 1998. [Online]. Available: <http://www.sciencedirect.com/science/article/pii/S0142112397000819>



DATONG WU received the Ph.D. degree from the University of Stuttgart, Germany. He is currently a Professor with the Department of Applied Sciences and Mechatronics, Munich University of Applied Sciences, Germany. His research interests include fiber-optic ultrasound transducers, photoacoustics, nanomaterials for photoacoustic applications, and advanced nondestructive material testing.



sensors, and memory cells.

JOHANNES JEHN received the B.Sc. and M.Sc. degrees in nanostructure technology from the University of Würzburg, Germany, in 2015 and 2018, respectively. He is currently pursuing the Ph.D. degree with INRS-EMT, Canada. Since Fall 2018, he has been with the Laboratory for Microsystems Technology, University of Applied Sciences, Munich, Germany. His research interests include fabrication, characterization, and integration of printed electronic components, such as batteries,



CHRISTIAN U. GROSSE received the Ph.D. degree from the University of Stuttgart, Germany. He currently holds the Chair of Non-destructive Testing as a Professor with the Technical University of Munich, Germany. His research interests include materials, such as concrete, metal, stone, and composites, such as fiber reinforced materials.



acoustic metamaterials for non-destructive materials engineering and medical imaging.

PATRICK OSER received the B.Eng. degree in precision engineering and mechatronics and the M.Eng. degree from the University of Applied Sciences, Munich, Germany, in 2015 and 2018, respectively. He is currently pursuing the Ph.D. degree with the Munich University of Applied Sciences in cooperation with the Technical University of Munich at the Chair of Non-Destructive Materials Testing Munich. His research topic is based on the synthesis and application of photoacoustic metamaterials for non-destructive materials engineering and medical



ULRICH MOOSHEIMER received the Diploma and Ph.D. degrees from the University of Regensburg. He is currently a Professor in printing technology with the University of Applied Sciences, Munich, Germany.



Society, Munich. His research interests include development and characterization of MEMS and printed electronic devices.

M. A. MAZ COURRAU received the B.Sc. degree in electronic engineering from the Colombian School of Engineering Julio Garavito, Bogota, Colombia, in 2014. He is currently pursuing the M.Sc. degree in micro and nanotechnology with the Munich University of Applied Sciences, Munich, Germany. From 2014 to 2018, he worked as an Access Network Engineer at Huawei, Bogota. He is working towards his master thesis with the Semiconductor Laboratory, Max Planck



ANDREAS RUEDIGER is currently a Professor with the Énergie Matériaux Télécommunications Research Centre, Varennes, QC, Canada.



MICHAEL KAISER received the Dipl.Ing. and M.Sc. degrees in microsystems technology from the University of Applied Sciences, Munich, Germany, in 1994 and 2008, respectively. Since early 1990, he has been working with the Laboratory for Microsystems Technology. His main research interests include semiconductor technology and the characterization of thin films and their optical properties.



CHRISTINA SCHINDLER received the Ph.D. degree from RWTH Aachen University, Aachen, Germany, in 2009. She is currently a Professor with the Hochschule München University of Applied Sciences, Germany and heading the Laboratory for Microsystems Technology. Her research interest includes resistive memories combined with printed electronics.

...